JACS
JOURNAL OF THE AMERICAN CHEMICAL SOCIETY

ARTICLE

pubs.acs.org/JACS

Probing Microscopic Architecture of Opaque Heterogeneous Systems Using Double-Pulsed-Field-Gradient NMR

Noam Shemesh, Tal Adiri, and Yoram Cohen*

School of Chemistry, The Raymond and Beverly Sackler Faculty of Exact Sciences, Tel Aviv University, Ramat Aviv, Tel Aviv 69978, Israel

Supporting Information

ABSTRACT: Microarchitectural features of opaque porous media and biological tissues are of great importance in many scientific disciplines ranging from chemistry, material sciences, and geology to biology and medicine. Noninvasive characterization of coherently organized pores is rather straightforward since conventional diffusion magnetic resonance methods can detect anisotropy on a macroscopic scale; however, it remains extremely challenging to directly infer on microarchitectural features on the microscopic scale in heterogeneous porous media and biological cells that are comprised of randomly oriented compartments, a scenario widely encountered in Nature. Here, we show that the angular bipolar double-pulsed-field-gradient (bp-d-PFG) methodology is capable of reporting on unique microarchitectural features of highly heterogeneous systems. This was demonstrated on a toluene-in-water emulsion system, quartz sand, and even biological specimens such as yeast cells and isolated gray matter. We find that in the emulsion and yeast cells systems, the angular bp-d-PFG methodology uniquely revealed nearly an image of the pore space, since it conveyed direct microarchitectural information such as compartment shape and size. In two different quartz sand specimens, the angular bp-d-PFG experiments demonstrated the presence of randomly oriented anisotropic compartments. We also obtained unequivocal evidence that diffusion in interconnected interstices is restricted and therefore non-Gaussian. In biological contexts, the angular bp-d-PFG experiments could uniquely differentiate between spherical cells and randomly oriented compartments in gray matter tissue, information that could not be obtained by conventional NMR methods. The angular bp-d-PFG methodology also performs very well even when severe background gradients are present, as is often encountered in realistic systems. We conclude that this method seems to be the method of choice for characterizing the microstructure of porous media and biological cells noninvasively.

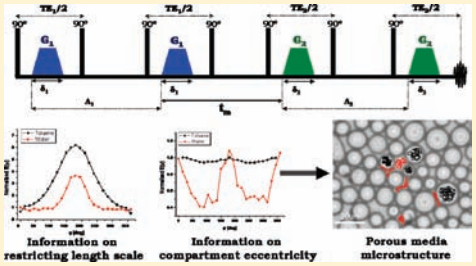

INTRODUCTION

Opaque porous systems are prevalent in a myriad of chemical[1] and biological[2] systems. In many cases, microarchitectural features such as pore size, shape, and organization may have profound effects on the physical, chemical, and even biological properties of the system, and therefore noninvasive determination of such microstructural properties is of paramount importance. Since the seminal paper of Stejskal and Tanner more than 55 years ago,[3] diffusion NMR has become by far the most important methodology for noninvasively characterizing pores in heterogeneous systems. The celebrated Stejskal−Tanner single-pulsed-field-gradient (s-PFG) methodology (Figure 1A) conveys microstructure by utilizing diffusion of endogenous magnetic resonance (MR)-observable nuclei as reporters for microarchitectural features of the porous systems. Indeed, diffusion NMR has been used to study systems such as heterogeneous catalysts,[4] porous polymers,[5] porous materials[6a−c] and carbon nanotubes,[6d] rocks,[7] emulsions[8a] and colloids,[8b] and even biological cells[9] and tissues.[10] In the past decade, *q*-space diffusion NMR,[11] originally designed to noninvasively study compartment size in chemical and biological systems, was extended to magnetic resonance imaging (MRI) and was used to provide micrometer-scale information on axons and fibers in the central nervous system (CNS).[12] All these systems were studied mostly using the s-PFG methodology, which is capable of characterizing pores directly only when the pores are coherently organized (Figure 1B), i.e., when the systems are characterized by organization on the macroscopic scale; such systems are in fact characterized by ensemble anisotropy (eA).[13]

However, in many systems in Nature, much more complex scenarios may prevail in which eA is not present, as shown in Figure 1C,D, for example. The scenario shown in Figure 1C, where anisotropic compartments are completely randomly oriented, can be found in many heterogeneous systems such as catalysts and porous polymers, and even in gray matter of the CNS. Another scenario where there is no macroscopic organization may be encountered when a solid matrix is immersed in fluid, as shown in Figure 1D. Despite the absence of eA, these scenarios can be still characterized by microscopic anisotropy (μA), which is a manifestation of the restriction length scale in the system, and compartment shape anisotropy (csA), which is a manifestation of the pore eccentricity.[13] However, s-PFG

Received: January 12, 2011
Published: March 29, 2011

dx.doi.org/10.1021/ja200303h | *J. Am. Chem. Soc.* 2011, 133, 6028–6035

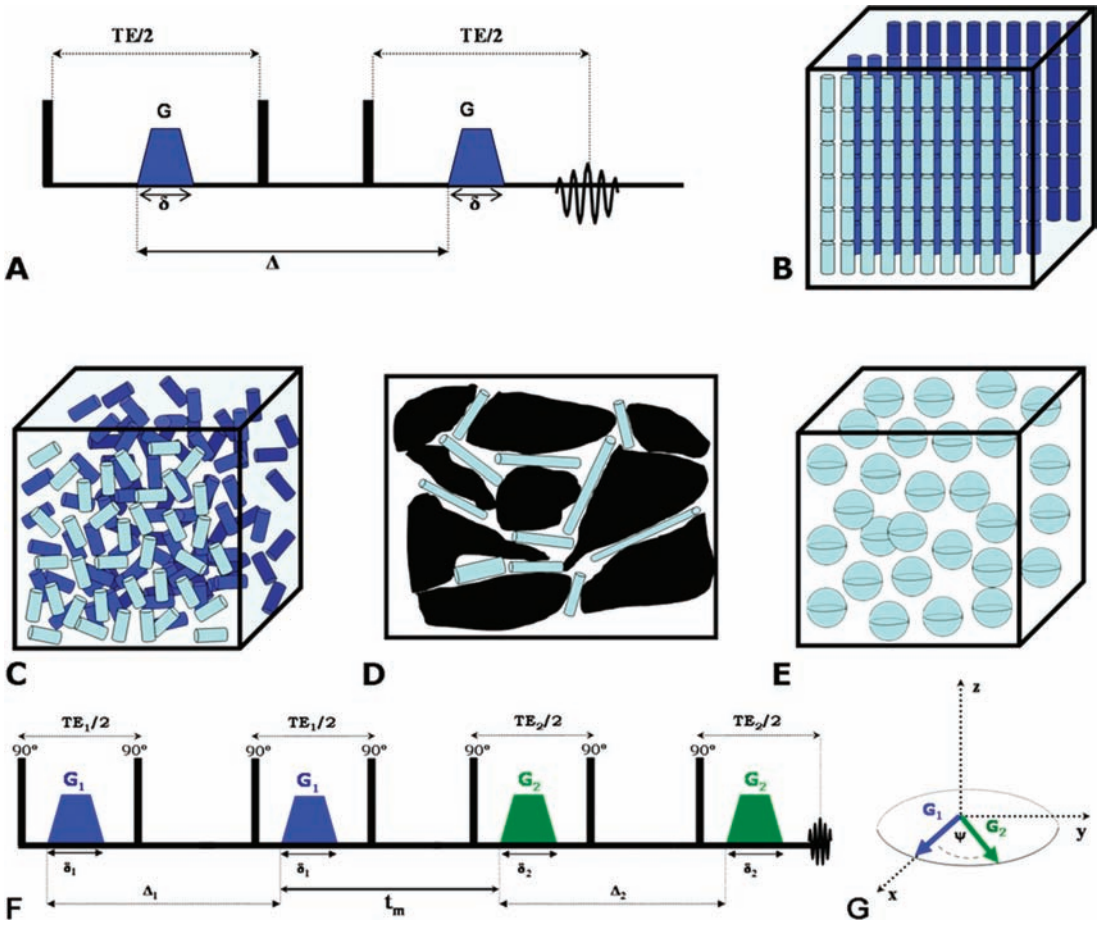

Figure 1. Sequences and schemes. (A) The Stejskal−Tanner single-PFG experiment. (B) The s-PFG experiments are capable of easily conveying microstructural information in coherently organized systems only, where ensemble anisotropy exists, which implies that diffusion is anisotropic on a macroscopic scale. (C−E) Scenarios that are all macroscopically isotropic: (C) randomly oriented anisotropic compartments, (D) diffusion in the interstices of a solid matrix, and (E) diffusion in spheres. In all of these cases, diffusion appears isotropic, and it is impossible to distinguish between these scenarios in s-PFG MR. (F) A double-PFG sequence. Note that two gradient pairs are applied in succession, with the timing between them defined as the mixing time (t_m). In this specific sequence, the case of $\psi = 180°$ is shown owing to the fourth and fifth 90° RF pulses. (G) The angular d-PFG methodology. Here, the gradient durations and amplitudess are set, along with the diffusion periods and the mixing time. What is varied is simply the relative angle between the gradient vectors, defined as ψ. Here, the experiment is shown in the $X-Y$ plane.

approaches are only capable of detecting eA, i.e., microstructure on a macroscopic scale, while they inherently cannot detect μA and csA. Therefore, using s-PFG approaches, it is difficult to distinguish between the scenarios shown in Figure 1C,D (i.e., randomly oriented anisotropic compartments) and perfectly isotropic spheres (Figure 1E).

In 1995, a theoretical work by Mitra claimed that a variant of double-PFG (d-PFG) NMR (a double-stimulated-echo variant is shown in Figure 1F), namely the angular d-PFG NMR experiment, should be able to accurately characterize systems such as those shown in Figure 1C−E.[14] The d-PFG sequence employs two independent gradient vectors $\mathbf{G_1}$ and $\mathbf{G_2}$, having durations δ_1 and δ_2, respectively, and spanning diffusion periods Δ_1 and Δ_2, respectively (Figure 1F). The advantage of the angular d-PFG MR methodology is that it utilizes two unique parameters that have no analogy in conventional s-PFG MR, namely the angle ψ between the two gradient vectors and the mixing time (t_m), which is defined as the duration between the two diffusion periods Δ_1 and Δ_2 (Figure 1F). In such experiments, the gradient amplitudes are set constant and equal, while the orientation of the second gradient vector $\mathbf{G_2}$ is rotated with respect to the direction of the first gradient vector $\mathbf{G_1}$ at a constant mixing time (Figure 1G; for a review on d-PFG, see ref 15). In angular d-PFG MR, the signal intensity is plotted as a function of ψ (hereafter referred to $E(\psi)$). Preceding the angular d-PFG experiments were nonangular double-PFG MR experiments designed to measure locally anisotropic motion in yeast cells,[16] liquid crystals,[17] gray matter of the CNS,[18] and even spinal cords.[19]

Recent theoretical studies claimed that the angular d-PFG MR experiments could distinguish between the scenarios shown in Figure 1C,D and the scenario shown in Figure 1E by inspecting the $E(\psi)$ at different mixing times.[13,14,20,21] In scenarios where eA is absent, the theory suggested that at $t_m = 0$ ms the $E(\psi)$ profile would be solely determined by μA and csA, giving rise to signatures in the form of bell-shaped functions in the $E(\psi)$ plots.[13,20] At long t_m however, μA is decoupled from the $E(\psi)$ profile, thus isolating the effects of csA on the angular profile, and potentially offering a means to distinguish between anisotropic compartments (giving rise to sharp modulations in $E(\psi)$) and spheres (where no modulation was predicted in $E(\psi)$).[13] The angular dependencies at short t_m were recently observed experimentally by both spectroscopy[22,23] and imaging.[24] Recently, we used controlled synthetic porous media to demonstrate for the

dx.doi.org/10.1021/ja200303h | J. Am. Chem. Soc. 2011, 133, 6028–6035

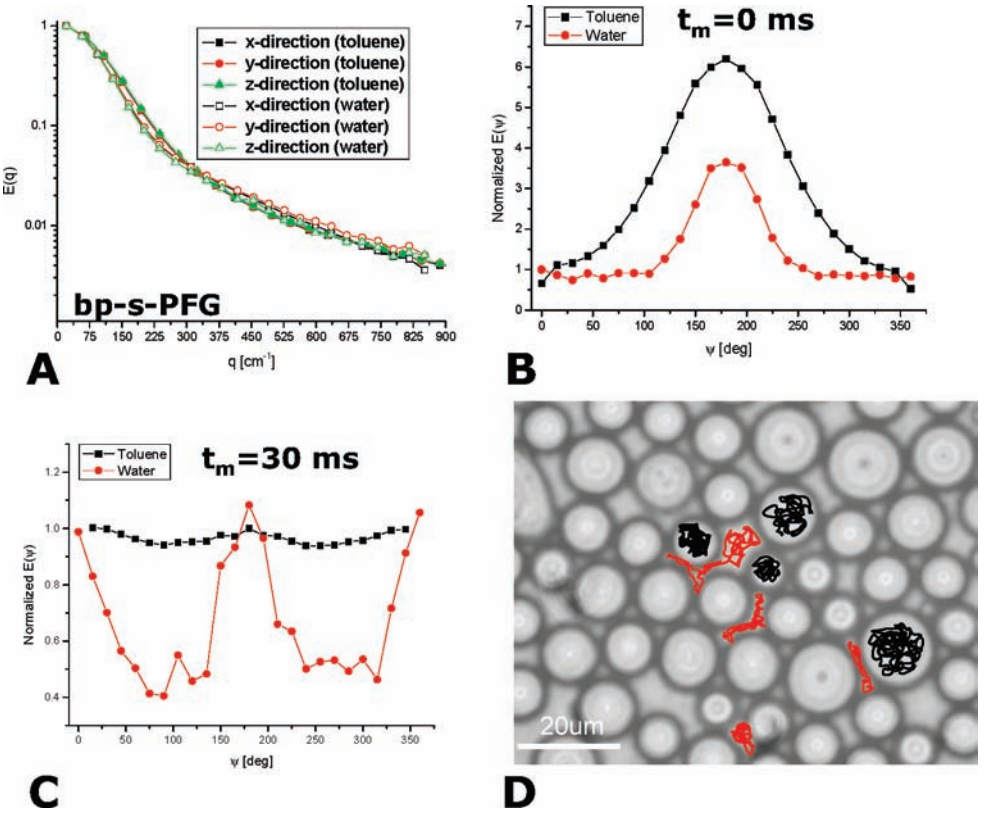

Figure 2. Insights into pore morphology in an emulsion system. (A) bp-s-PFG experiments conducted on both the toluene and water resonances. The signal attenuation in all directions is very similar, and it is difficult to differentiate between the two components on the basis of these diffusion profiles. (B) Angular bp-d-PFG experiments with t_m = 0 ms in the same emulsion. The microscopic anisotropy of both components is clearly revealed, and it is clear that the water component is more restricted than the toluene. (C) The angular bp-d-PFG experiments with long mixing time reveal that the toluene molecules diffuse in spherical compartments, while water molecules are diffusing in highly anisotropic, randomly oriented compartments. (D) The invasive light microscopy shows the spherical toluene droplets dispersed in water. The water is confined to smaller pores that are highly anisotropic in shape (red), albeit randomly oriented. The bp-d-PFG experiments are therefore capable of uniquely depicting the microstructure of the emulsion. Bp-d-PFG experiments were performed at $2q$ = 460 cm^{-1}.

first time that the angular bipolar-d-PFG (bp-d-PFG) experiments at long t_m can indeed offer signatures for compartment eccentricity, even in the scenario shown in Figure 1C.[23]

In this study, for the first time, we study realistic, complex specimens that possess both microstructural heterogeneity and large magnetic inhomogeneity, and in some cases even interconnection, using the angular d-PFG methodology. We sought to study whether d-PFG can indeed describe the pore morphology, especially in those scenarios where conventional methods are inherently limited. We show that the angular bp-d-PFG (sequences shown in Figure S2) methodology indeed offers unique and novel signatures for underlying microstructure in highly heterogeneous systems, such as emulsions, quartz sand, and even biological specimens such as yeast cells and CNS gray matter, that could not be obtained from the conventional diffusion MR methods. This is obtained completely noninvasively and using relatively weak gradient amplitudes.

RESULTS AND DISCUSSION

Toluene-in-Water Emulsion. One of the most important applications of diffusion NMR in general is in characterizing the microstructure of emulsion systems.[25] In the NMR spectrum of an oil-in-water emulsion consisting of toluene droplets dispersed in water, the water and oil peaks were well resolved on the chemical shift axis. We could therefore compare the microstructural information available from conventional bp-s-PFG MR measurements to microstructural information that could be obtained from angular bp-d-PFG experiments. Figure 2A shows the bp-s-PFG diffusion NMR measurements conducted on the resonances of both the toluene methyl peak and the water peak in this emulsion in three orthogonal directions. The signal decays in the *x*-, *y*-, and *z*-directions are practically identical for both materials, suggesting that there is no eA within this specimen. Interestingly, the $E(q)$ signal decays of both H_2O and toluene appear quite similar, and it can only be inferred from bp-s-PFG MR that diffusion is not mono-Gaussian for both peaks, but this in itself does not indicate physical restriction or any underlying microstructural features in the emulsion. For example, a similar non-mono-Gaussian profile could be a result of two distinct populations of a diffusing moiety having different molecular weights but the same chemical shift; in such cases, the higher and lower molecular weight moiety will have two different Gaussian propagators, which will produce a non-mono-Gaussian signal decay in the $E(q)$ plot. The bp-s-PFG MR experiments in this specimen therefore imply only that both toluene and water components are diffusing in macroscopically isotropic environments (vide infra).

By contrast, the bp-d-PFG experiments reveal a completely different picture for both of the emulsion components. At t_m = 0 ms, pronounced bell-shaped $E(\psi)$ dependencies are observed

dx.doi.org/10.1021/ja200303h |*J. Am. Chem. Soc.* 2011, 133, 6028–6035

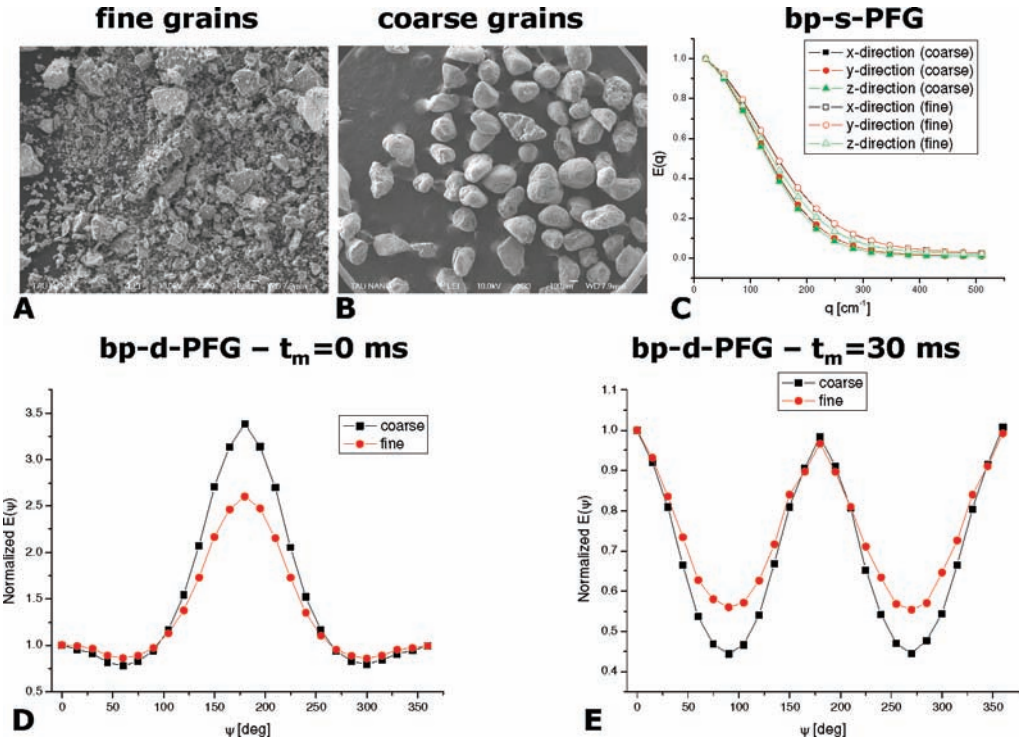

Figure 3. Experiments in quartz sand specimens. (A) SEM image of the specimen that was crushed to fine grains. (B) SEM image of the specimen where sand grains were large. (C) Bipolar s-PFG experiments for both specimens, showing almost no differences between specimens, and the signal decay is almost isotropic in both specimens. (D) Angular bp-d-PFG experiments with t_m = 0 ms, showing effects of microscopic and compartment shape anisotropies in the normalized $E(\psi)$ plots. (E) Angular bp-d-PFG experiments with a long t_m of 30 ms in which the microscopic anisotropy is decoupled from the $E(\psi)$ plots, yielding a modulation that is dependent only on compartment shape anisotropy. The bp-d-PFG MR results are shown for $2q$ = 230 cm^{-1}.

for both components (Figure 2B), indicating that physical restriction is present for both components. Note that here, the normalized $E(\psi)$ dependencies are plotted to enable easy comparison between the components, and that the bell-shaped angular dependence will only arise from restricted, non-Gaussian diffusion (as opposed to multi-Gaussian diffusion processes).[14] Several implications arise from these $E(\psi)$ plots. First, the appearance of bell-shaped $E(\psi)$ dependencies directly implies that diffusion is restricted and non-Gaussian for both water and toluene components of the emulsion. Second, since the magnitude of the bell-shaped function is dependent on pore size,[14] the $E(\psi)$ plots suggest that each component is restricted by a different geometrical scale: remarkably, the data in Figure 2B show that the angular dependence of water is *smaller* than that of toluene, suggesting that water molecules are in fact confined to smaller domains compared to toluene molecules. This unique signature for compartment size, however, is not sufficient to completely characterize the pore space, as information on pore shape is not completely resolved in the t_m = 0 ms experiments.

To directly infer on underlying compartment shape, experiments were performed using long t_m.[13,23] Figure 2C shows these experiments for the toluene resonance: a flat $E(\psi)$ profile is obtained, suggesting that csA is very small for toluene. This means that toluene is in fact diffusing within a restricting isotropic, spherical compartment. By contrast, a remarkable modulation is observed for the water peak, suggesting that water molecules are diffusing in a network of randomly oriented nonspherical compartments. Combined with the information from the t_m = 0 ms experiments that show that water molecules diffuse in smaller compartments compared to toluene, the angular bp-d-PFG MR completely conveys the underlying microstructure in the emulsion: toluene is diffusing in large spherical droplets that create confining anisotropic regions that are smaller in size, where water molecules are experiencing restricted diffusion between the droplets. Indeed, under invasive light microscopy (Figure 2D), the toluene droplets appear spherical, suggesting that toluene molecules are experiencing restricted diffusion (black lines) on a larger scale than water molecules (red lines), which undergo restricted, non-Gaussian diffusion in smaller, locally anisotropic, randomly oriented compartments.

Since the toluene droplets were found to be spherical in the long t_m experiment, compartment size could be estimated. The size that was extracted for the toluene droplets was 17.2 ± 0.2 μm. This is in reasonable agreement with the sizes observed in microscopy (Figure 2D). However, it should be noted that a substantial size distribution exists in the emulsion, and therefore the size extracted at this q-value probably represents a weighted average of the globules present.

While the bell-shaped $E(\psi)$ curve for toluene clearly follows the expected cosine profile, the $E(\psi)$ profile of water exhibits a much narrower, non-cosine peak that we could not fit to Mitra's theory.[14] The non-cosine profile most likely arises from the superposition of csA effects (that were indeed clearly revealed in the long t_m regime). Since these pores appear to be interconnected, new theory that will take into account exchange effects and restriction on different length scales is needed for future quantification of the μA effects. Nevertheless, the angular bp-d-PFG

dx.doi.org/10.1021/ja200303h |*J. Am. Chem. Soc.* 2011, 133, 6028–6035

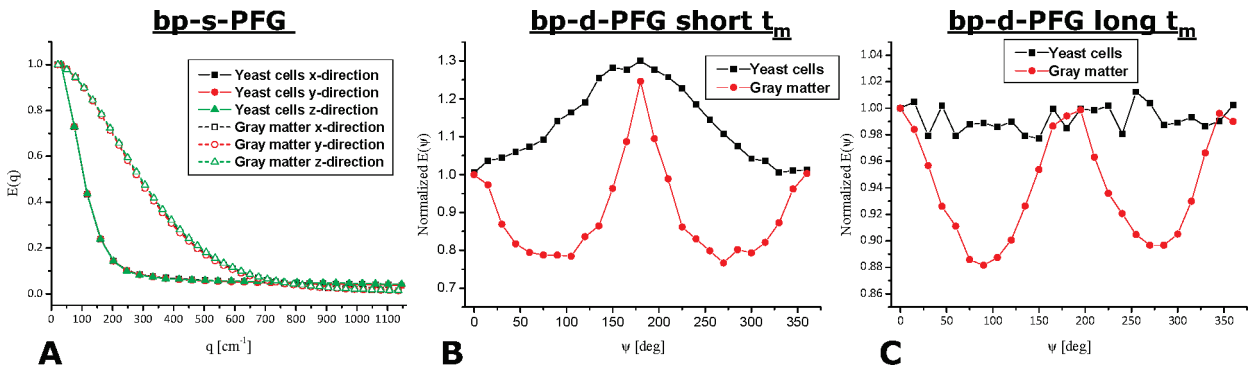

Figure 4. Experiments in isotropic biological systems. (A) Bipolar-s-PFG experiments in yeast cells and in gray matter (Δ/δ = 200/3 and 50/3, respectively). Note the completely isotropic signal decay in both specimens. (B) Angular bp-d-PFG experiments at t_m = 0 ms for both specimens, showing markedly different $E(\psi)$ dependencies. Note the smooth bell-shaped profile in the yeast cells, compared to the marked modulated $E(\psi)$ curve in gray matter. (C) Angular bp-d-PFG experiments with long t_m, showing the different compartment shapes. In yeast cells, the $E(\psi)$ plot is completely flat, indicating that the cells are spherical, while in the gray matter, a pronounced modulation remains in the $E(\psi)$ plots, indicating that diffusion occurs in randomly oriented, restricted anisotropic compartments. All angular bp-d-PFG experiments were performed at $2q$ = 1384 cm^{-1}.

experiments at both t_m regimes uniquely provided nearly an image of the emulsion microstructure.

Quartz Sand Specimens. Noninvasive characterization of microstructure is extremely important in petrochemical research, where characterizing diffusion in rocks or between sand grains is related to oil content and transport properties.[7] We therefore applied bp-s-PFG and angular bp-d-PFG to two quartz sand specimens which have very different sand grains: the first specimen had small, dust-like fine grains, while the second specimen had coarse grains that are much larger. Figure 3A,B shows the scanning electron microscopy (SEM) images of these specimens. Note that here, the porous network is in fact the interstices *between* the grains (as shown in Figure 1C). The SEM images reveal the Achilles' heel of invasive microscopy, as the sand microstructure cannot be probed in its native state (maximally packed).

Figure 3C shows the bp-s-PFG experiments conducted on both specimens in the *x*-, *y*-, and *z*-directions. In both specimens, diffusion appears to be almost completely isotropic in bp-s-PFG experiments. Furthermore, the diffusion attenuation of both specimens appears quite similar, so that a "fingerprint" for the sand microstructure is very elusive. The isotropic profiles of the bp-s-PFG experiments in fact indicate that for these specimens, eA is not present; i.e., diffusion is macroscopically isotropic. However, inferring on restricted, non-Gaussian diffusion from these plots is elusive, and whether the non-mono-Gaussian profile arises from restriction or from multi-Gaussian processes cannot be inferred from the data without resorting to diffusion time dependence of the signal decay.

Figure 3D shows the angular bp-d-PFG experiments at t_m = 0 ms in both specimens using weak gradients. Several striking observations can be made. In both specimens, clear bell-shaped functions were observed. These are the first observations of bell-shaped functions in sand specimens using bp-d-PFG NMR, and they provide several basic insights into the specimen microstructure: μA is revealed in both specimens; furthermore, the bell-shaped functions unequivocally imply that diffusion is restricted and non-Gaussian, even at low q-values for the experimental parameters used, since bell-shaped functions at t_m = 0 ms will arise solely from restricted diffusion, as opposed to multi-Gaussian processes.[14]

Another important feature of these plots is that the percent change in $E(\psi)$ in the specimen where grains are larger is higher than in the second specimen, where grains are ground to smaller sizes. The signal increases by up to 340% in the coarse grains, while in the fine grains the signal increases by "only" 260%. Therefore, Figure 3D shows that the restricted diffusion length scale between the larger grains is indeed larger on average than the diffusion length scale between the smaller grains.

The angular bp-d-PFG experiments conducted at long mixing times are shown in Figure 3E. A pronounced modulation of the normalized $E(\psi)$ plots can be clearly seen in both specimens, indicating the presence of csA; note that $E(\psi = 180°) \approx E(\psi = 0°)$, as predicted by the theory.[13] Furthermore, the modulation is stronger in coarse grains, suggesting that the eccentricity of the compartments that are restricting the diffusion between the grains is larger in the coarse grains. These new fingerprints that the angular bp-d-PFG experiment reveals, namely microscopic and compartment shape anisotropies, therefore provide a multitude of novel microstructural information in these highly heterogeneous specimens. Since diffusion of endogenous fluid may be an indicator of transport properties within the porous media, such noninvasive characterization can be extremely important in petrochemical applications.

Biological Specimens. Diffusion MR methods are extensively used in biological and medical applications, and especially in the CNS.[2] By far, s-PFG approaches and especially diffusion tensor imaging (DTI) have been most widely used owing to their ability to portray anisotropic diffusion in the white matter of the CNS, where the white matter fibers are coherently organized and are characterized by eA on the macroscopic scale. However, the s-PFG approaches yield almost no information in the gray matter, where diffusion appears macroscopically isotropic;[18] therefore, s-PFG approaches are inherently limited in characterizing such regions, and information on the microscopic scale is very elusive. Gray matter is comprised of cell bodies, which are rather spherical in size, and dendrites and randomly oriented axons, which can be described, to a good approximation, as randomly oriented cylinders. We therefore conducted both bp-s-PFG and angular bp-d-PFG experiments in two biological specimens that are characterized by very different underlying microstructures: yeast cells that are spherical under light microscopy (data not shown) and an isolated pig gray matter specimen.

The bp-s-PFG MR experiments, conducted in the *x*-, *y*-, and *z*-directions, are shown in Figure 4A. Note that for each specimen, a different diffusion time was used. The signal decay for both

dx.doi.org/10.1021/ja200303h |*J. Am. Chem. Soc.* 2011, 133, 6028–6035

specimens is completely isotropic and non-mono-Gaussian, revealing little insight into the compartment shape, and the multi-Gaussian decay does not indicate directly on restriction. The angular bp-d-PFG experiments (Figure 4B), on the other hand, show a markedly different picture: the yeast cells clearly reveal a bell-shaped $E(\psi)$ profile, indicating the μA experienced by the intracellular water, while a markedly different $E(\psi)$ plot is revealed in the gray matter. The modulation in the $E(\psi)$ profile of gray matter in fact arises from the coupling of μA and csA.[13] To decouple the effects of μA, we performed the angular bp-d-PFG experiments at long t_m. Again, marked contrast between the two specimens is clearly observed. A flat, ψ-independent $E(\psi)$ profile is obtained for the yeast cells, indicating that water is confined within isotropic, spherical compartments. Indeed, under invasive light microscopy, the cells appeared spherical (data not shown). By contrast, in the gray matter, a $\cos(2\psi)$ modulation is observed, which indicates that water is confined in randomly oriented compartments that are locally anisotropic (Figure 4C). Such novel microstructural information on the compartment shape is expected to play an important role and substantiate MR imaging of gray matter tissues using underlying microstructural information as a new source of contrast. For example, areas rich in cell bodies may have smaller eccentricities (that will manifest as smaller modulations at long t_m), while areas richer in dendrites, for example, may show a stronger modulation of the $E(\psi)$ plots. Nevertheless, the csA as well as μA in gray matter could also arise from other compartments such as glial cells, extracellular matrix, and even water diffusing in connective tissues. Further studies will be needed to elucidate the role of each biological constituent on the modulation of the $E(\psi)$ plots and therefore on the underlying microstructure that is reported via the angular bp-d-PFG MR noninvasively. However, it seems that the angular bp-d-PFG NMR experiments do have the potential to provide signatures for the different compartment shapes, as is demonstrated in the spherical yeast cells. Since the yeast cells were found to be spherical in the long t_m experiments, we could attempt to fit a compartment size to the restricted $E(\psi)$ profile at $2q = 942$ cm^{-1}, the extracted size was 3.6 ± 0.1 μm, which is slightly smaller than the cell size observed in microscopy (approximately 5 μm, data not shown). This deviation is likely an artifact of the finite gradient pulses and the timings between the bipolar gradients.

One of the important attributes of angular d-PFG MR experiments is that they allow one to unequivocally infer on the presence of restricted, non-Gaussian diffusion within an opaque system. In s-PFG MR, diffusion−diffraction patterns[26a] in $E(q)$ data are also unequivocal evidence for the presence of restricting boundaries and therefore can be used as reporters for microstructure; however, these diffraction patterns are rapidly lost owing to size[22c] or orientation[23] distributions. In such scenarios, restricted diffusion can still be probed by s-PFG MR, to a certain extent, when $E(q)$ data are acquired as a function of Δ.[7a,26b] The dependence of the extracted apparent diffusion coefficient (ADC) on the diffusion time can be used to infer on restriction.[7a,26b] Furthermore, the Fourier transform of the $E(q)$ data using the q-space approach results in probability distribution functions (PDFs), which can be used to extract root-mean-squared displacements (rmsd's) of the components.[11,12,27] There, the Δ-dependence of the rmsd's can also be used as an indication on restriction. To study the possibility of inferring on restriction from s-PFG experiments, Δ-dependent q-space experiments were performed in the yeast cells specimen (Figure S3A). Indeed, the PDFs at the different Δ's are clearly non-mono-Gaussian, revealing that more than a single diffusion mode exists (Figure S3B). When rmsd's were extracted from the PDFs and plotted against $\Delta^{1/2}$, a slow component that was restricted to about 4 μm was observed; this component was diffusion time independent for the values of Δ used. A fast component was also extracted, which was clearly found to have a linear dependence on $\Delta^{1/2}$, as expected from Gaussian diffusion (Figure S3C). The Δ-independence of the slow component suggests that restricted diffusion occurs in the yeast cells; however, a multi-Gaussian propagator is not necessarily indicative of restriction imposed by physical boundaries and would also emerge from multi-Gaussian processes. Therefore, detecting the bell-shaped curves in $E(\psi)$ angular d-PFG MR experiments appears to be advantageous, as they can only be a result of physical restriction, thus providing direct and conclusive evidence for physical restriction and μA. Furthermore, $E(\psi)$ data can be acquired much more rapidly compared to densely sampled $E(q)$ data at multiple Δs using the s-PFG MR methodology.

CONCLUSIONS

To conclude, this study demonstrates that angular bp-d-PFG MR experiments can noninvasively provide unique insights into pore morphology and organization, even in extremely heterogeneous systems that cannot be characterized using conventional methods. Insights into underlying microstructure on the micrometer scale were obtained in systems ranging from oil-in-water emulsions to fluid in between quartz sand grains, and even in biological systems such as yeast cells and CNS gray matter. In all of these systems, the conventional bp-s-PFG methods could only report on macroscopic effects and altogether missed much of the rich underlying microstructural information that could be obtained from the angular bp-d-PFG experiments. In all cases, restricted, non-Gaussian diffusion was directly detected using the angular bp-d-PFG methodology, and the restricting length scales as well as the compartment shape could be accurately inferred.

We note that the methodology is rather easy to implement, and that in most cases it can be used under rather mild experimental conditions. Furthermore, the angular bp-d-PFG MR sequences have proven useful even when very large magnetic inhomogeneity was present (as is generally encountered in many porous materials, rocks, catalysts, etc.; in several of our specimens, line widths of over 1000 Hz were encountered and successfully overcome). Furthermore, these results suggest that applying angular bp-d-PFG in MR imaging could provide new sources of contrast based on underlying microstructural properties, thus offering new ways of imaging porous media in general and biological specimens such as the gray matter in the CNS in particular. It therefore seems that the angular bp-d-PFG MR methodology could indeed be of great value for studying opaque porous chemical and biological systems. Efforts are underway to extend these findings to d-PFG MR imaging.

EXPERIMENTAL SECTION

Specimen Preparation. The toluene emulsion was prepared by dissolving 40 μL of Triton X-100 (Sigma Aldrich, Rehovot, Israel) in 1980 μL of H_2O and subsequently adding 1980 μL of toluene. The mixture was vortexed for several seconds and allowed to separate. The upper turbid emulsion was aspirated, placed in a 5 mm NMR tube, and allowed to equilibrate for several hours prior to the NMR experiments. No further phase separation was observed in the NMR tube, even after

several days. The line width in these specimens was ~30 Hz for the methyl peak of toluene and ~200 Hz for the water peak.

The quartz sand specimens were prepared as follows. One specimen of clean coarse quartz sand grains was placed in a 10 mm NMR tube. Distilled water was poured until the entire sample was wet, and then the NMR tube was sealed. A second specimen was prepared where the coarse quartz sand was initially mechanically crushed to smaller dust-like particles. The crushed grains were placed in a 10 mm NMR tube, which was then filled with distilled water similarly to the previous specimen. The specimens were allowed to equilibrate for several days prior to the NMR experiment. In the coarse grains the line width was ~700 Hz, while in the fine grains the line width was ~1200 Hz.

The yeast cells specimen was prepared as follows. The yeast was hydrated with phosphate-buffered saline (PBS) and then centrifuged for 10 min at 1000 rpm. The yeast was then suspended in paraformaldehyde (Sigma-Aldrich) fixative for 90 min and washed twice with PBS (Sigma-Aldrich). After the second wash, the cells were centrifuged again for 10 min at 1000 rpm. The supernatant was removed, and the yeast cells were suspended in a small amount of PBS, which was poured into an 8 mm NMR tube. The fixated cells were allowed to settle overnight at 4 °C, and the water that collected above the yeast was removed prior to the NMR experiments. The line width in the yeast cells specimen was ~50 Hz.

The gray matter was prepared using a fixated pig brain (Lahav, Israel) that was washed twice with PBS and then sliced into coronal, sagittal, and axial slices from which gray matter could be clearly visualized. Using a scalpel, gray matter pieces were scraped from the pig brain (without any attempt to isolate a specific gray matter region), and care was taken not to include any white matter in the specimen. The gray matter was placed in a 10 mm NMR tube filled with Fluorinert, and the tube was stoppered using an 8 mm NMR tube filled with Fluorinert. The line width in the gray matter was ~40 Hz.

NMR Experiments. The NMR tube containing each specimen was placed in a Bruker 8.4 T NMR spectrometer equipped with a Micro5 probe capable of producing nominal pulsed gradients up to 1900 mT/m in each direction. The temperature was kept constant throughout the experiments.

In the angular d-PFG experiments, the angle between the two gradient vectors, ψ, is varied and the signal intensity $E(\psi)$ is measured. To do so, the direction of the first gradient vector $\mathbf{G_1}$ is fixed, and the direction of the second gradient vector $\mathbf{G_2}$ is varied with respect to the fixed direction of $\mathbf{G_1}$. In this study, all angular d-PFG and bp-d-PFG MR experiments were performed using the following methodology: $\mathbf{G_1}$ was fixed in the x-direction, and the orientation of $\mathbf{G_2}$ was varied in 25 equal steps along 360° in the $X-Y$ plane (perpendicular to the direction of $\mathbf{B_0}$), resulting in 25 ψ-values. In all angular d-PFG and bp-d-PFG experiments in this study, $|\mathbf{G_1}| = |\mathbf{G_2}|$, i.e., $|\mathbf{q_1}| = |\mathbf{q_2}|$ ($|\mathbf{q}| = (2\pi)^{-1}\gamma\delta|\mathbf{G}|$, where $\mathbf{G}$ is the gradient wave vector). For a review on the d-PFG methodology, see ref 15.

Microscopy Experiments. The quartz sand grains were imaged using a High-resolution scanning electron microscope (HRSEM, JEOL 6700F operated at 15 KeV) equipped with a secondary electron detector.

Experimental Parameters for NMR Experiments: Toluene-in-Water Emulsion System. The bp-s-PFG MR experiments were performed using the sequence shown in Figure S1, with $\Delta/\delta = 200/3$ ms. The angular bp-d-PFG experiments were performed with the bipolar sequence shown in Figure S2B with the parameters $\Delta_1 = \Delta_2 = 150$ ms, $\delta_1 = \delta_2 = \delta_3 = 3$ ms, and $t_m = 0$ ms, and with the bipolar sequence shown in Figure S2A with the parameters $\Delta_1 = \Delta_2 = 150$ ms, $\delta_1 = \delta_2 = 3$ ms, and $t_m = 30$ ms.

Quartz Sand Specimens. The bp-s-PFG MR experiments were performed using the sequence shown in Figure S1, with $\Delta/\delta = 200/3$ ms. The angular bp-d-PFG experiments were performed with the bipolar sequence shown in Figure S2B with the parameters $\Delta_1 = \Delta_2 = 250$ ms, $\delta_1 = \delta_2 = \delta_3 = 2$ ms, and $t_m = 0$ ms, and with the bipolar sequence shown in Figure S2A with the parameters $\Delta_1 = \Delta_2 = 250$ ms, $\delta_1 = \delta_2 = 2$ ms, and $t_m = 30$ ms.

Biological Specimens. In the yeast cells, bp-s-PFG MR experiments were performed using the sequence shown in Figure S1, with $\Delta/\delta = 200/3$ ms. The bipolar angular d-PFG experiments at short t_m were performed with the sequence shown in Figures S2B with the parameters $\Delta_1 = \Delta_2 = 60$ ms, $\delta_1 = \delta_2 = \delta_3 = 3$ ms, and $t_m = 0$ ms. The bipolar angular d-PFG experiments at long t_m were performed with the sequence shown in Figures S2A with the parameters $\Delta_1 = \Delta_2 = 60$ ms, $\delta_1 = \delta_2 = 3$ ms, and $t_m = 15$ ms.

The q-space experiments in the yeast cells were performed using an s-STE sequence. Ninety-six q-values were acquired for $\Delta = 50$, 100, 150, 250, and 400 ms, resulting in five $E(q)$ data sets. In all data sets, $\delta = 2$ ms, and the maximum gradient was 1600 mT/m, yielding a maximum q-value of 1362 cm^{-1}. Each $E(q)$ data set was Fourier transformed, and the resulting probability distribution function was fitted to a bi-Gaussian function, from which the rmsd of each component was extracted.

In the gray matter, bp-s-PFG MR experiments were performed using the sequence shown in Figure S1, with $\Delta/\delta = 50/3$ ms. The bipolar angular d-PFG experiments at short t_m were performed with the sequence shown in Figures S2B with the parameters $\Delta_1 = \Delta_2 = 50$ ms, $\delta_1 = \delta_2 = \delta_3 = 3$ ms, and $t_m = 0$ ms. The bipolar angular d-PFG experiments at long t_m were performed with the sequence shown in Figures S2A with the parameters $\Delta_1 = \Delta_2 = 50$ ms, $\delta_1 = \delta_2 = 3$ ms, and $t_m = 28$ ms.

Size Extraction. Where pores are not obviously interconnected (for which theory does not exist), we attempted to extract a compartment size from the $E(\psi)$ plots. The data at $t_m = 0$ ms for the toluene component of the emulsion and the yeast cells were fitted at a single q-value to the simplified expression for restricted diffusion in spheres in Özarslan's paper[13] (eq 25a in ref 13), to which another free-diffusion compartment was added to compensate for the overall signal attenuation.[22b]

■ ASSOCIATED CONTENT

Supporting Information. Supporting Figures S1, S2, and S3, with captions. This material is available free of charge via the Internet at http://pubs.acs.org

■ AUTHOR INFORMATION

Corresponding Author
ycohen@post.tau.ac.il

■ ACKNOWLEDGMENT

Y.C. and N.S. were partially supported by the CONNECT consortium administered by the European commission under Framework Package 7. N.S. gratefully acknowledges the Clore Scholars Program for a scholarship. N.S. thanks Dr. Peter Basser and Dr. Evren Özarslan from the National Institutes of Health for stimulating discussions. Y.C., T.A., and N.S. thank Prof. Aldo Shemesh from the Weizmann Institute of Science for the quartz sand specimens.

■ REFERENCES

(1) (a) Blumich, B. *NMR imaging of materials*; Clarendon: Oxford, 2009. (b) Kärger, J., Michel, D., Eds. *Magn. Reson. Chem.* **1999**, *37*, S1−S159.

(2) Johansen-Berg, H.; Behrens, T., Eds. *Diffusion MRI: From quantitative measurement to in-vivo neuroanatomy*; Academic Press: New York, 2009.

(3) Stejskal, E. O.; Tanner, J. E. *J. Chem. Phys.* **1965**, *42*, 288–292.

(4) Valiullin, R.; Naumov, S.; Galvosas, P.; Kärger, J.; Woo, H. J.; Porcheron, F.; Monson, P. A. *Nature* **2006**, *443*, 965–968.

(5) Kuntz, J. F.; Trausch, G.; Palmas, P.; Mutzenhardt, P.; Canet, D. *J. Chem. Phys.* **2007**, *126*, 134904.

(6) (a) Kukla, V.; Kornatowski, J.; Demuth, D.; Gimus, I.; Pfeifer, H.; Rees, L. V. C.; Schunk, S.; Unger, K. K.; Kärger, J. *Science* **1996**, *272*, 702–704. (b) Tallarek, U.; van Dusschoten, D.; Van As, H.; Guiochon, G.; Bayer, E. *Angew. Chem., Int. Ed.* **1998**, *37*, 1882–1885. (c) Tallarek, U.; Rapp, E.; Van As, H.; Bayer, E. *Angew. Chem., Int. Ed.* **2001**, *40*, 1684–1687. (d) Marega, R.; Aroulmoji, V.; Dinon, F.; Vaccari, L.; Giordani, S.; Bianco, A.; Murano, E.; Prato, M. *J. Am. Chem. Soc.* **2009**, *131*, 9086–9093.

(7) (a) Hurlimann, M. D.; Helmer, K. G.; Latour, L. L.; Sotak, C. H. *J. Magn. Reson. A* **1994**, *111*, 169–178. (b) Song, Y. Q.; Ryu, S. G.; Sen, P. N. *Nature* **2000**, *406*, 178–181.

(8) (a) Goudappel, G. J. W.; van Duynhoven, J. P. M.; Mooren, M. M. W. *J. Colloid Interface Sci.* **2001**, *239*, 535–542. (b) Valentini, M.; Vaccaro, A.; Rehor, A.; Napoli, A.; Hubbell, J. A.; Tirelli, N. *J. Am. Chem. Soc.* **2004**, *126*, 2142–2147.

(9) (a) Kuchel, P. W.; Coy, A.; Stilbs, P. *Magn. Reson. Med.* **1997**, *37*, 637–643. (b) Tang, X. P.; Sigmund, E. E.; Song, Y. Q. *J. Am. Chem. Soc.* **2004**, *126*, 16336–16337.

(10) Basser, P. J.; Mattiello, J.; Lebihan, D. *Biophys. J.* **1994**, *66*, 259–267.

(11) (a) Callaghan, P. T.; Macgowan, D.; Packer, K. J.; Zelaya, F. O. *J. Magn. Reson.* **1990**, *90*, 177–182. (b) Cory, D. G.; Garroway, A. N. *Magn. Reson. Med.* **1990**, *14*, 435–444.

(12) (a) Cohen, Y.; Assaf, Y. *NMR Biomed.* **2002**, *15*, 516–542. (b) Ong, H. H.; Wehrli, F. W. *Neuroimage* **2010**, *51*, 1360–1366.

(13) Özarslan, E. *J. Magn. Reson.* **2009**, *199*, 56–67.

(14) Mitra, P. P. *Phys. Rev. B* **1995**, *51*, 15074–15078.

(15) Shemesh, N.; Özarslan, E.; Komlosh, M. E.; Basser, P. J.; Cohen, Y. *NMR Biomed.* **2010**, *23*, 757–780.

(16) (a) Cheng, Y.; Cory, D. G. *J. Am. Chem. Soc.* **1999**, *121*, 7935–7936. (b) Cory, D. G.; Garroway, A. N.; Miller, J. B. *Polym. Prepr.* **1990**, *31*, 149–150.

(17) Callaghan, P. T.; Komlosh, M. E. *Magn. Reson. Chem.* **2002**, *40*, S15–S19.

(18) Komlosh, M. E.; Horkay, F.; Freldlin, R. Z.; Nevo, U.; Assaf, Y.; Basser, P. J. *J. Magn. Reson.* **2007**, *189*, 38–45.

(19) Komlosh, M. E.; Lizak, M. J.; Horkay, F.; Freidlin, R. Z.; Basser, P. J. *Magn. Reson. Med.* **2008**, *59*, 803–809.

(20) (a) Özarslan, E.; Basser, P. J. *J. Chem. Phys.* **2008**, *128*, 154511. (b) Özarslan, E.; Shemesh, N.; Basser, P. J. *J. Chem. Phys.* **2009**, *130*, 104702.

(21) (a) Koch, M. A.; Finsterbusch, J. *Magn. Reson. Med.* **2009**, *62*, 247–254.(b) Lawrenz, M.; Koch, M. A.; Finsterbusch, J. *J. Magn. Reson.* **2009**, *202*, 43−56.

(22) (a) Shemesh, N.; Özarslan, E.; Basser, P. J.; Cohen, Y. *J. Magn. Reson.* **2009**, *198*, 15–23. (b) Shemesh, N.; Özarslan, E.; Bar-Shir, A.; Basser, P. J.; Cohen, Y. *J. Magn. Reson.* **2009**, *200*, 214–225. (c) Shemesh, N.; Özarslan, E.; Basser, P. J.; Cohen, Y. *J. Chem. Phys.* **2010**, *132*, 034703.

(23) Shemesh, N.; Özarslan, E.; Adiri, T.; Basser, P. J.; Cohen, Y. *J. Chem. Phys.* **2010**, *133*, 044705.

(24) (a) Koch, M. A.; Finsterbusch, J. *Magn. Reson. Med.* **2008**, *60*, 90–101. (b) Weber, T.; Ziener, C. H.; Kampf, T.; Herold, V.; Bauer, W. R.; Jakob, P. M. *Magn. Reson. Med.* **2009**, *61*, 1001–1006.

(25) Johns, M. L.; Hollingsworth, K. G. *Prog. Nucl. Magn. Reson. Spectrosc.* **2007**, *50*, 51–70.

(26) (a) Callaghan, P. T.; Coy, A.; Macgowan, D.; Packer, K. J.; Zelaya, F. O. *Nature* **1991**, *351*, 467–469. (b) Sen, P. N. *Concepts Magn. Reson. A* **2004**, *23A*, 4–21.

(27) (a) Bar-Shir, A; Avram, L; Özarslan, E; Basser, P. J.; Cohen, Y. *J. Magn. Reson.* **2008**, *194*, 230–236. (b) Topgaard, D.; Söderman, O. *Magn. Reson. Imaging* **2002**, *21*, 69–76.